Title: **InGaAs/InP SPAD detecting single photons at 1550 nm with up to 50% efficiency and low noise**

Authors: F. Signorelli; F. Telesca; E. Conca; A. Della Frera; A. Ruggeri; A. Giudice; A. Tosi

Publisher: IEEE

DOI Link: https://doi.org/10.1109/IEDM19574.2021.9720559

Citation format:

F. Signorelli et al., "InGaAs/InP SPAD detecting single photons at 1550 nm with up to 50% efficiency and low noise," 2021 IEEE International Electron Devices Meeting (IEDM), 2021, pp. 20.3.1-20.3.4, doi: 10.1109/IEDM19574.2021.9720559.

InGaAs/InP SPAD detecting single photons at 1550 nm with up to 50% efficiency and low noise

F. Signorelli[1], F. Telesca[1], E. Conca[1], A. Della Frera[2], A. Ruggeri[2], A. Giudice[2] and A. Tosi[1]
[1] Dipartimento di Elettronica, Informazione e Bioingegneria, Politecnico di Milano, 20133 Milano, Italy,
email: fabio.signorelli@polimi.it
[2] Micro Photon Devices Srl, 39100 Bolzano, Italy

***Abstract*—** We present an InGaAs/InP single-photon avalanche diode (SPAD) with high photon detection efficiency and low noise for fiber-based quantum optics applications. Compared to previous InGaAs/InP SPADs, the InGaAs absorption layer is thicker, to maximize the quantum efficiency. The double zinc diffusion has been adjusted to avoid premature edge breakdown, with the help of a guard ring structure. Our detector achieves a photon detection efficiency up to 50% at 1550 nm, with a dark count rate of 20 kcps and a timing jitter of ~ 70 ps (FWHM) at 225 K. Alternatively, it features a photon detection efficiency of 37% at 1550 nm, with a dark count rate of just 3 kcps and a timing jitter of ~ 100 ps (FWHM). When combined with a custom integrated circuit, afterpulsing probability is as low as few percent with a gating frequency of 1 MHz and hold-off time of few microseconds at 225 K, allowing to achieve a photon count rate of almost 1 Mcps.

I. Introduction

Detectors with high photon detection efficiency (PDE) in the short-wavelength infrared range (SWIR) are required by many applications, from light detection and ranging (LiDAR) [1] to quantum optics applications [2], such as quantum communications and quantum computers. Among all the available SWIR single-photon detectors, InGaAs/InP single-photon avalanche diodes (SPADs) feature the typical advantages of solid-state detectors, such as low cost, high reliability, compactness, and ease of use, together with good overall performance. However, performance of InGaAs/InP SPADs still need to be improved, especially in terms of PDE and maximum photon count rate.

Here, we present the design and experimental characterization of a new InGaAs/InP SPAD with enhanced photon detection efficiency and low noise, with a maximum count rate up to 1 Mcps.

II. Detector Structure

Our detector has an active area diameter of 10 µm, suitable for a high coupling efficiency pigtailing with a single-mode fiber via a single-lens focusing system. The internal structure of our InGaAs/InP SPADs is shown in Fig. 1, while a micrograph of the die is reported in Fig. 2.

Aiming at enhancing the photon detection efficiency, the new device features a thicker (2 µm) InGaAs absorption region. With the support of TCAD simulations, carried out both with a commercially-available software and custom algorithms, we optimized the internal structure of the SPAD, in order to avoid premature edge breakdown and mitigate possible non-uniformities inside the active area, which could arise due to the thicker depleted region (see simulations in Fig. 3). Specifically, we adjusted the shape and depth of the double zinc diffusion and tuned the doping inside the charge layer to tailor the electric field inside the device for noise reduction. However, lowering the electric field in the absorber worsens the charge persistence phenomenon [3]. To avoid edge breakdown and reduce charge persistence, we added a modified guard ring structure, which is contacted through a dedicated metal pad (see Fig. 2): the guard ring can be biased at the voltage needed to contrast charge persistence by increasing the local electric field underneath.

III. Experimental Results

The InGaAs/InP SPADs were experimentally tested by operating them in gated-mode, where a square wave biases the detector from below to above the breakdown voltage. The excess bias (V_{EX}) is the difference between the bias voltage and the breakdown level.

A. I-V Characteristics

Fig. 4 shows the I-V characteristics of the SPAD at 225 K, including both dark current and photo-current (when illuminated with laser at 1550 nm). The breakdown voltage is clearly at ~ 68 V, while the punch-through voltage, i.e. when the depleted region reaches the InGaAs layer, is ~ 53 V. The dark current below breakdown is not meaningful for SPAD operation, since contributions from the surface, which might be significant, do not get multiplied and do not contribute to DCR.

B. Photon Detection Efficiency

We measured the PDE of our InGaAs/InP SPAD by focusing a CW laser at 1550 nm inside the active area of the detector, after properly attenuating it at the single-photon level. The laser spot size is ~ 5 µm, which is similar to what obtained in a fiber-pigtailed system where a SMF-28 optical fiber coupled to the SPAD by means of a single lens. Fig. 5 shows the DCR as a function of PDE (corresponding excess bias values are also reported). Fig. 6 shows a 2D map of the PDE at different excess bias voltages. At V_{EX} = 3 V, PDE non-uniformities inside the active area are clearly visible, while at V_{EX} = 7 V and 9 V they are much attenuated as the avalanche triggering probability tends to saturate at high V_{EX}.

C. Guard Ring bias

Fig. 7 shows DCR when changing the bias voltage ΔV_{GR-A} between the guard ring and the SPAD anode, for three different V_{EX}. If a too small ΔV_{GR-A} voltage is applied, edge breakdown occurs near the guard ring and, as consequence, DCR is worsened: the device behaves like a wider SPAD, as if the guard ring were part of the shallow diffusion. If, instead, a too high ΔV_{GR-A} voltage is applied, the guard ring has no longer an influence in suppressing edge effects, so DCR increases due to premature edge breakdown (as for a structure with no guard ring). However, there is an optimal ΔV_{GR-A} voltage range that ensures a correct SPAD operation, i.e. when the guard ring slightly influences the electric field in the layers beneath, so to reduce DCR and charge persistence. If the guard ring is left floating, its electric potential results from the structure and its applied voltages, but it does not minimize DCR, as it can be seen from the dashed lines in Fig. 7. All measurements of this work, apart from Fig. 7, are acquired with the optimal ΔV_{GR-A}.

D. Dark Count Rate

Fig. 8 shows the dark count rate measured at different temperatures and different excess bias voltages. The gate period is kept long enough (100 µs) to ensure that no afterpulsing is present. At the typical operating temperature of 225 K (reached by a 3-stage thermo-electric cooler mounted inside a TO-8 package), we measured a DCR as low as just few kcps. When the temperature is lowered to 200 K, DCR increases when $V_{EX} > 7$ V due to the dominating charge persistence effect, while at even lower temperatures DCR decreases again, thanks to a strongly reduced carrier generation. At 300 K, DCR is ~ 200 kcps and 400 kcps at V_{EX} of 3 V and 5 V, respectively.

E. Afterpulsing

Afterpulsing probability has been characterized by wire bonding our SPAD to a front-end integrated circuit that we specifically designed to swiftly quench the avalanche in a very short time (~ 1 ns) for optimizing the detector performance. The integrated circuit has been manufactured in a 0.16 µm BCD technology and is capable of gating and quenching up to 8 SPADs independently at a maximum excess bias of 5 V. The front-end circuit is based on a differential SPAD-DUMMY readout to reject common-mode disturbances and allow gate windows as short as 2 ns, and has been designed to operate at 225 K very close to the detectors (see Fig. 9). We calculated the afterpulsing probability with the TCCC technique [4]: Fig. 10 shows the results as a function of hold-off time, at two different excess bias voltages and gating frequencies. Fig. 11 shows an example of interarrival time histogram: afterpulsing becomes negligible (i.e. < 0.01%) with hold-off times greater than 50 µs, while we measured just 0.3% with 20 µs hold-off time and 4% with 5 µs hold-off time at $V_{EX} = 5$ V and 1 MHz of gate frequency. Additionally, preliminary measurements at higher temperatures (275 K) show a strong reduction of the afterpulsing probability. Further investigations are currently in progress.

F. Timing jitter

A pulsed laser (18 ps FWHM) at 1550 nm has been focused inside the active area of the SPAD, with the same setup employed for PDE measurements. Fig. 12 shows the instrument response function, acquired with a standard TCSPC setup. Our SPAD features a narrow timing response, ranging from 72 ps at $V_{EX} = 11$ V to 319 ps at 3 V excess bias. Fig. 13 shows timing measurements acquired at different points inside the active area for investigating the secondary peak present just after the main one at high V_{EX}. As the relative amplitude of the two contributions changes with the position inside the active area, we can conclude that it is due to residual non-uniformities in the avalanche triggering probability inside the active area.

IV. Conclusions

We presented a InGaAs/InP SPAD with enhanced photon detection efficiency for fiber-based quantum applications. We designed a thicker absorption layer, along with an improved zinc diffusion and a fine-tuned charge layer. Optimizing the guard ring voltage, our detector exhibits a PDE up to 50% at 1550 nm with few kpcs DCR at a temperature of 225 K, and a narrow timing jitter of ~ 70 ps (FWHM). Afterpulsing is strongly reduced, thanks to a dedicated integrated circuit we designed to this purpose, to values as low as few percent at 225 K. Table 1 compares the performance of our InGaAs/InP SPAD with similar detectors recently described in literature: our detector has state-of-the-art PDE with low dark count rate.

Acknowledgments

This work was partially funded by the Autonomous Province of Bozen/Bolzano with the SPIR project (Bando Innovazione 2016).

References

[1] A. M. Pawlikowska, A. Halimi, R. A. Lamb, and G. S. Buller, "Single-photon three-dimensional imaging at up to 10 kilometers range," *Opt. Express*, vol. 25, no. 10, p. 11919, May 2017.

[2] R. H. Hadfield, "Single-photon detectors for optical quantum information applications," *Nature Photonics*, vol. 3, no. 12. Nature Publishing Group, pp. 696–705, Dec. 01, 2009.

[3] N. Calandri, M. Sanzaro, A. Tosi, and F. Zappa, "Charge Persistence in InGaAs/InP Single-Photon Avalanche Diodes," *IEEE J. Quantum Electron.*, vol. 52, no. 3, Mar. 2016.

[4] S. Cova, A. Lacaita, and G. Ripamonti, "Trapping Phenomena in Avalanche Photodiodes on Nanosecond Scale," *IEEE Electron Device Lett.*, vol. 12, no. 12, pp. 685–687, 1991.

[5] S.-H. Baek, S.-C. Yang, C.-Y. Park, C.-W. Park, S.-B. Cho, and S.-W. Ryu, "Room temperature quantum key distribution characteristics of low-noise InGaAs/InP single-photon avalanche diode," *J. Korean Phys. Soc. 2021 787*, vol. 78, no. 7, pp. 634–641, Mar. 2021.

[6] C.-Y. Park, C. Park, S.-K. Han, S.-B. Cho, and S. Baek, "Dual anode single-photon avalanche diode for high-speed and low-noise Geiger-mode operation," *Opt. Express, Vol. 27, Issue 13, pp. 18201-18209*, vol. 27, no. 13, pp. 18201–18209, Jun. 2019.

[7] Y. Tamura *et al.*, "Development of InGaAs MPPC for NIR photon counting applications," *Proc. SPIE, Optical Components and Materials XV*, Feb. 2018, p. 35.

[8] T. Baba *et al.*, "Development of an InGaAs SPAD 2D array for flash LIDAR," *Proc. SPIE, Quantum Sensing and Nano Electronics and Photonics XV*, vol. 10540, no. 26, p. 105400L, Jan. 2018.

[9] X. Jiang *et al.*, "InGaAsP/InP Geiger-mode APD-based LiDAR," *Proc. SPIE, Optical Sensing, Imaging, and Photon Counting: From X-Rays to THz*, vol. 10729, p. 107290C, Sep. 2018.

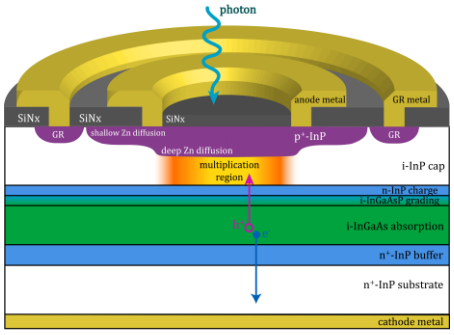

Fig. 1. Cross-sectional diagram of the front-illuminated InGaAs/InP SPAD here presented. Layers and doping regions are labeled in the picture.

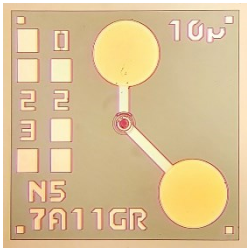

Fig. 2. Micrograph of the fabricated InGaAs/InP SPAD (chip frontside). The two round bonding pads contact the anode (bottom right) and the guard ring (top center), while the cathode is contacted from the backside (not visible here).

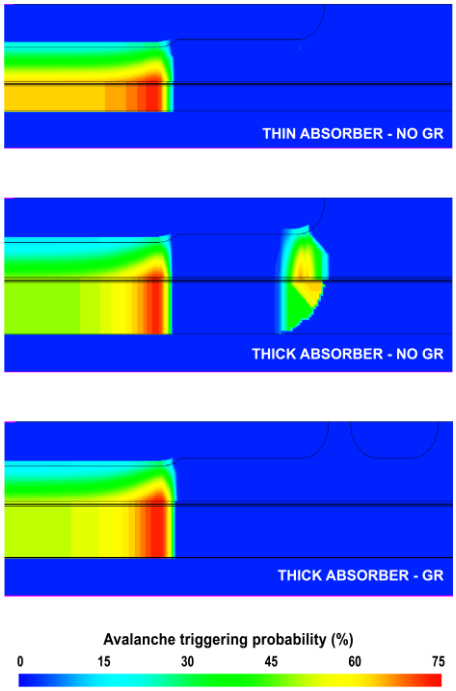

Fig. 3. Examples of avalanche triggering probability TCAD simulations for InGaAs/InP SPADs with thin and thick absorber. A guard ring is needed for the thicker structure to avoid edge breakdown. Only half of the detector is represented.

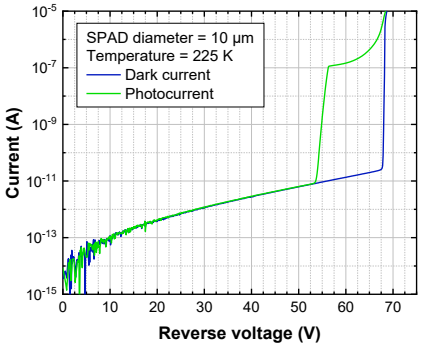

Fig. 4. Current-voltage characteristics at 225 K. Photocurrent is acquired while illuminating the device with 1550 nm photons.

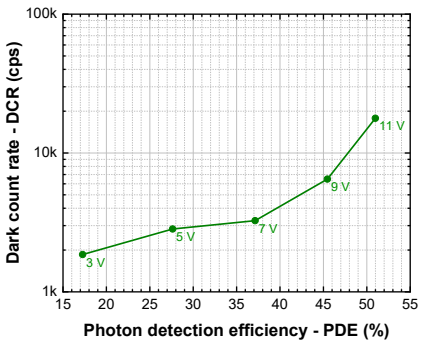

Fig. 5. Dark count rate as a function of the photon detection efficiency at different excess bias voltages. Temperature is 225 K.

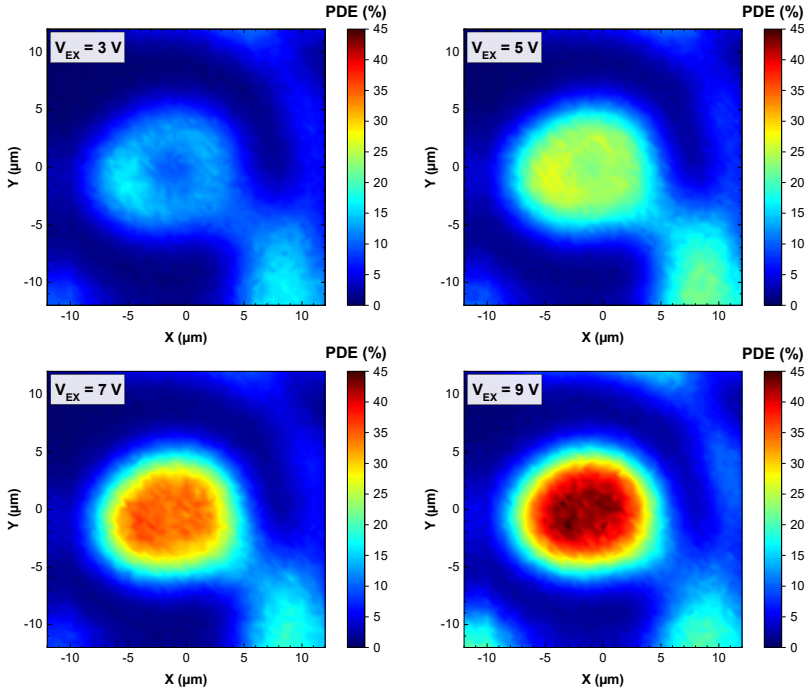

Fig. 6. 2D maps of photon detection efficiency at different excess bias voltages. The scale is the same for all the graphs. The images show minor distortions due to positioning issues when the laser spot is scanned by means of a xyz motorized micro-positioning system.

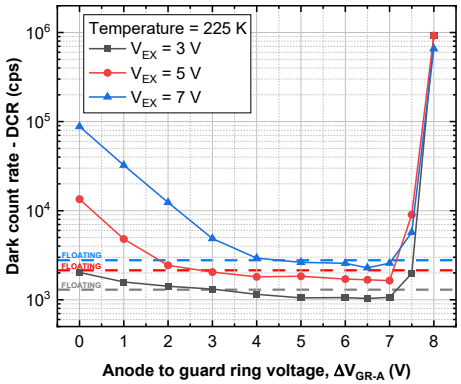

Fig. 7. Dark count rate as a function of the bias voltage $\Delta V_{GR\text{-}A}$ between the guard ring and SPAD anode, at different excess bias voltages. DCR values when the guard ring is left floating are reported as dashed horizontal lines. Temperature is 225 K.

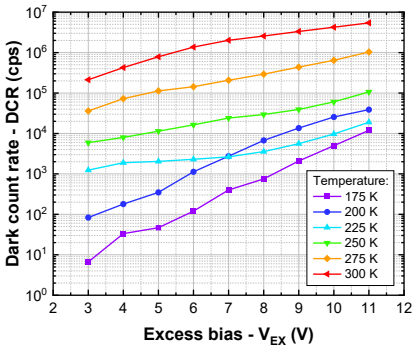

Fig. 8. Dark count rate as a function of the excess bias voltage at different operating temperatures.

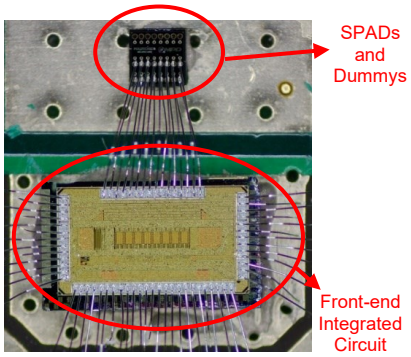

Fig. 9. Micrograph of the front-end integrated circuit mounted onto a custom printed circuit board and directly wire bonded to our InGaAs/InP SPADs.

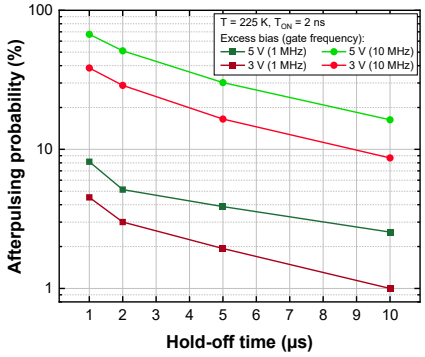

Fig. 10. Afterpulsing probability as a function of hold-off time, calculated with TCCC technique at different V_{EX} and gate frequencies.

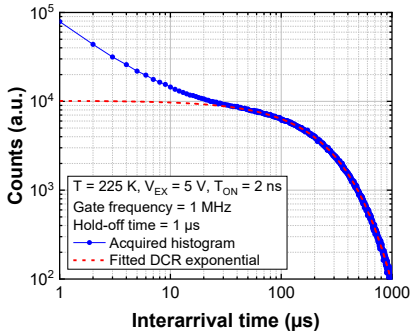

Fig. 11. Example of acquired inter-time histogram. The exponential curve (dashed line) is the fitting of the acquired histogram for interarrival times between 100 µs and 1000 µs, thus corresponding to the distribution of just primary DCR. The difference between the acquired curve and the fitted one is due to afterpulsing.

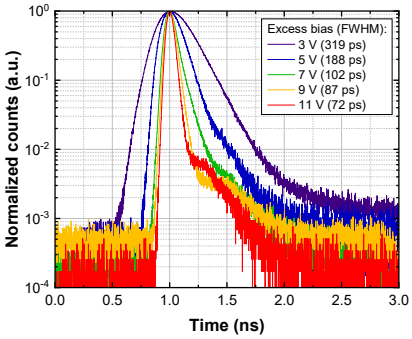

Fig. 12. Instrument response function at different excess bias voltages, acquired with a laser (18 ps, 1550 nm) focused inside the SPAD active area. Temperature is 225 K.

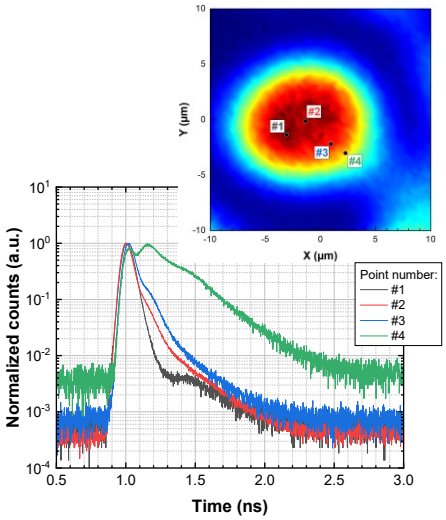

Fig. 13. Instrument response function at different locations across the SPAD active area, measured with V_{EX} = 9 V and at 225 K. The inset shows the positions of the different measurements.

Table 1 – Comparison of our detector with similar ones recently described in literature.

Reference	**This work**	[5]		[6]	[7]		[8]	[9]
Year	**2021**	2021		2019	2018		2018	2018
Nominal active area diameter [µm]	**10**	16		N.A.	9		12	N.A.
Temperature [K]	**225**	233	293	235	233	253	242	253
DCR [cps] @ PDE [%]	**1.9 k – 18 k @ 17.3 – 51**	4 k [a] @ 31	100 k [a] @ 31	168 k[b] @ 25.3	22 k[c] @ 10[d]	111 k @ 8[d]	234 @ 10	3.2 k @ 25
Afterpulsing probability [%] @ Hold-off time [ns][e]	**4.5 – 8.1 @ 1000**	2 – 7[f]	1 – 2.5[f]	0.7 – 21.6 @ 160	61.5 – 90	47 – 85	14.2 @ 800	10 – 25
Timing jitter [ps] @ PDE[a] [%]	**319 – 72 @ 17.3 – 51**	N.A.		N.A.	450 – 400 @ 10 – 50	580 – 450 @ 8 – 17	260[g]	190

[a] Computed from dark count probability per gate, with gate frequency = 10 MHz, gate width = 2 ns. [b] Computed from dark count probability per gate, with gate frequency = 1 GHz, gate width = 400 ps. [c] DCR of the single pixel computed as 1/9th of the DCR of a 3×3 array. [d] Afterpulse probability not subtracted. [e] When available. [f] Changes with gate signal amplitude. [g] Measurement conditions: T = 255 K, V_{EX} = 1.6 V.